J. Chem. Sci. Vol. 126, No. 2, March 2014, pp. 517–525.

Synthesis and visible light photocatalytic activity of nanocrystalline $PrFeO_3$ perovskite for hydrogen generation in ethanol–water system

S N TIJARE[a], S BAKARDJIEVA[b], J SUBRT[b], M V JOSHI[a], S S RAYALU[a], S HISHITA[c] and NITIN LABHSETWAR[a,*]

[a]CSIR - Network Institute of Sustainable Energy (CSIR-NISE), CSIR-National Environmental Engineering Research Institute (CSIR-NEERI), Nagpur 440 020, India

[b]Institute of Inorganic Chemistry, Academy of Sciences of the Czech Republic, Rez., Prague, Czech Republic

[c]National Institute for Materials Science, 1-1Namiki, Tsukuba, Ibaraki 305-0044, Japan

e-mail: nk_labhsetwar@neeri.res.in

MS received 18 November 2013; revised 9 January 2014; accepted 10 January 2014

Abstract. Nanocrystalline $PrFeO_3$ perovskite type orthoferrite was synthesized at 700°C by using three different synthesis methods, namely sol–gel, template and combustion method. The synthesized materials were characterized by XRD, BET-SA, SEM, HRTEM, XPS, FTIR and UV-DRS techniques to understand their physico-chemical properties. Characterization data reveal the formation of nanocrystalline $PrFeO_3$ perovskite composition with improved physical properties, possibly due to lower synthesis temperature used. $PrFeO_3$ synthesized by sol–gel method consists of crystallite size of about 20 nm with absorption maxima at 595 nm wavelength in visible light range. This photocatalyst shows hydrogen generation of about 2847 μmol.g^{-1}.h^{-1}, under visible light irradiation in ethanol–water system. The photocatalyst was further investigated for various operational parameters such as photocatalyst dose variation, illumination intensity, time, etc. in a view to optimize the hydrogen generation as well as to understand mechanistic aspects. This material appears to follow a semiconductor type mechanism for ethanol-assisted visible light photocatalyic water-splitting and can also be an interesting candidate to develop hetero-junction type photocatalysts.

Keywords. Perovskite; $PrFeO_3$; photocatalyst; water-splitting; hydrogen.

1. Introduction

Hydrogen has long been recognized as one of the most potential alternatives to carbon-based fossil fuels, due to its high recyclability and near-zero carbon emission.[1,2] Fossil fuels are not enough to meet the forever growing demand for energy in future and also responsible for atmospheric pollution. Hydrogen has low energy content by volume but very high energy content among the common and futuristic fuels by weight.[3] Hence, extensive efforts are being made all over the world to develop various ways to produce hydrogen from a variety of existing resources.[4–8] Environment-friendly hydrogen generation techniques were preferred to overcome related environmental impacts[9] and therefore, it received great attention as an option to help meet future energy demands, as well as environmental obligations.[10] Consequently several attempts have been made towards hydrogen generation using photocatalytic water-splitting approach, which is one of the best ways among the renewable sources.[11–15] Mixed metal oxides including spinals and perovskites are also among the large category of materials being explored for photocatalytic water-splitting.[16,17] Perovskites are very stable, crystalline compounds with highly flexible compositions offering good possibilities to tailor their properties.[18] Use of perovskites and mixed oxides is also in focus due to their redox properties and abilities towards photocatalytic hydrogen generation,[19,20] as well as to use them in development of hetero-junction type materials with improved photocatalytic properties.

Iron oxide semiconductors and other iron-based catalytic and photocatalytic materials are very eye-catching due to their environmentally safe properties, abundance, low cost and nontoxic nature. Hence, iron-based perovskites, double perovskites type structures are also being considered interesting for possible improvement in catalytic properties of iron. However, relatively few reports are available on ferrite type compounds such as MFe_2O_4,[21] $LaFeO_3$,[22] $ZnFe_2O_4$[23] and $NiFe_2O_4$[24] for their photocatalytic activity including

*For correspondence

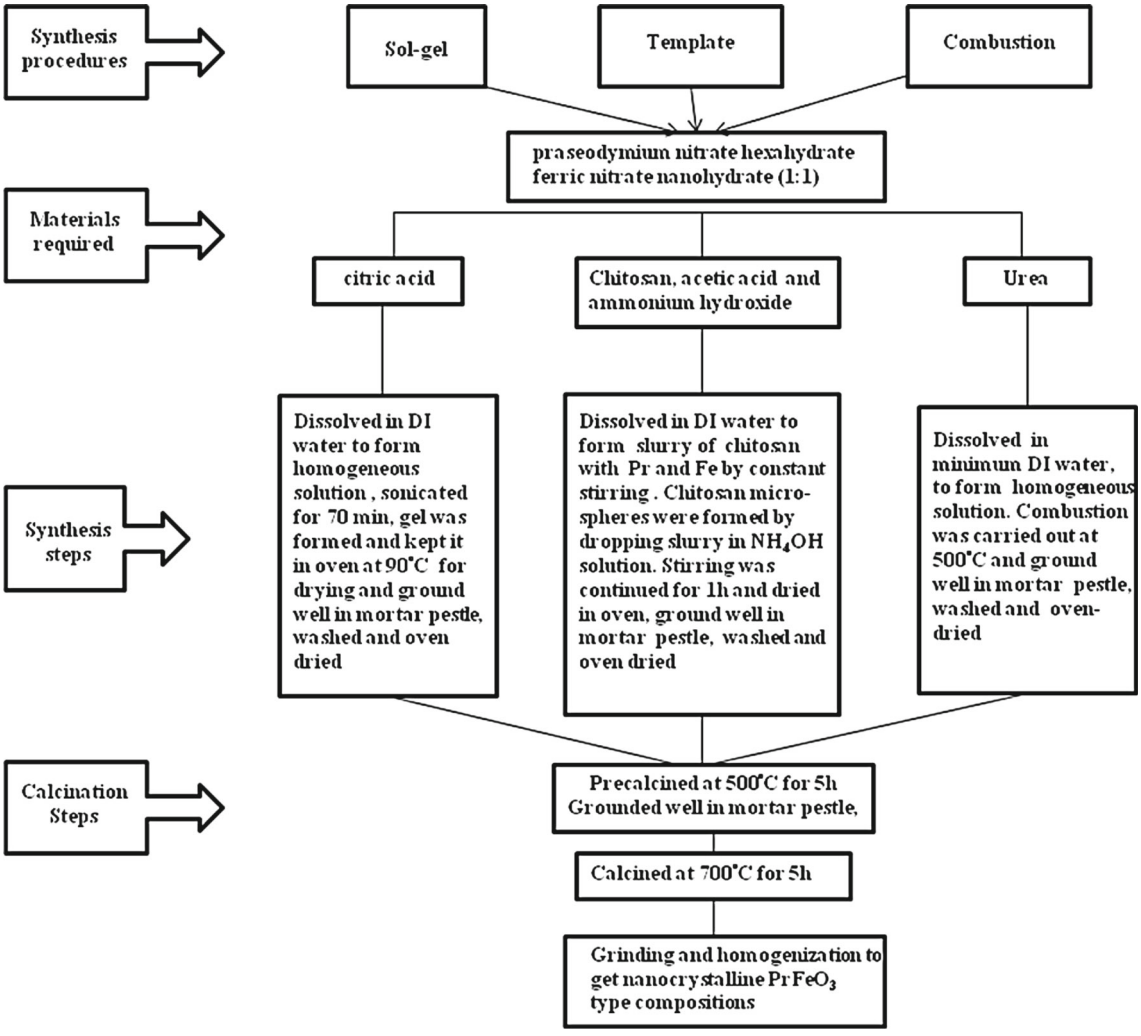

Figure 1. Synthesis of praseodymium ferrite by different synthesis routes.

hydrogen generation through water-splitting. In addition, it is also of interest to study iron-based rare earth perovskites and impact of particular rare earth metal on electronic and photocatalytic properties of ferrites. Oudenhoven *et al*. have nicely discussed the impact of rare earth elements through spinal structures,[11] however, there remains some ambiguity about the behaviour of such materials and this demands more investigations. With this background, iron-based $PrFeO_3$ perovskite was synthesized by using different methods and their photocatalytic properties were studied for hydrogen generation through alcohol-assisted water-splitting reaction. $LaFeO_3$ type perovskite with reasonably good photocatalytic hydrogen generation has already been reported by our group,[25] while we are extending this study to praseodymium ferrite, which was otherwise widely studied for its ferroelectric and ferromagnetic properties.[26,27] To the best of our knowledge, $PrFeO_3$ perovskite has so for not been explored systematically for photocatalytic hydrogen generation through water-splitting.

2. Experimental

2.1 *Materials*

The following chemicals were used for the synthesis of praseodymium ferrite photocatalysts: praseodymium nitrate hexahydrate (SIGMA-ALDRICH), ferric nitrate nanohydrate, acetic acid and citric acid (e-MERCK Mumbai India), Urea A.R. (HIMEDIA, Mumbai, India), chitosan (Chemchito, India) and ammonium hydroxide (25% NH_3) (Qualigens, India). All the chemicals were of analytical grade and used without further purifications. Deionized water was used as solvent for all the syntheses.

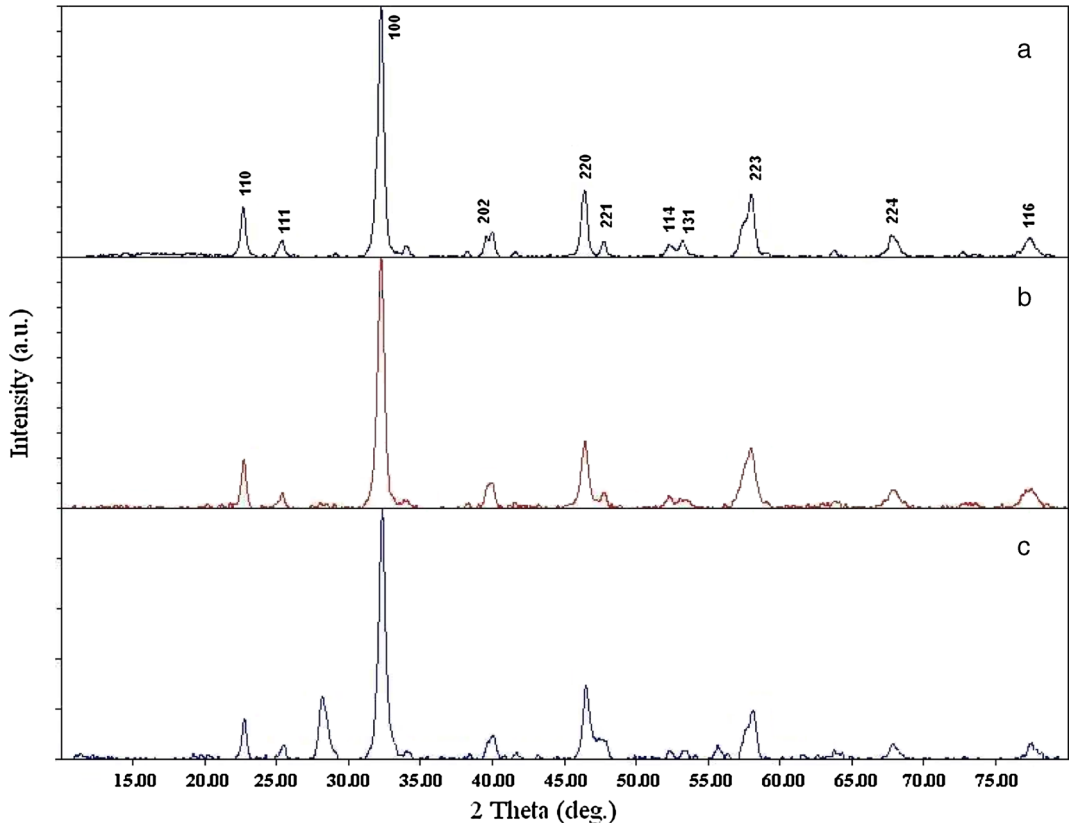

Figure 2. XRD patterns for $PrFeO_3$ perovskite synthesized by various methods at 700°C (**a** sol-gel, **b** chitosan template and **c** combustion).

2.2 *Methods of synthesis*

Praseodymium ferrite type photocatalysts were synthesized by using three different synthetic routes namely sol–gel, template and combustion; and the same is discussed as follows.

In sol–gel synthesis method, $Pr(NO_3)_3.6H_2O$ (8.7 g), $Fe(NO_3)_3.9H_2O$ (8.08 g) and citric acid (7.7 g) were used. Chitosan (6 g) was used along with Pr (8.7 g), and Fe (8.08 g) precursor in template method. However, in case of combustion synthesis, urea (2.4 g) was used with $Pr(NO_3)_3.6H_2O$ (8.7 g) and $Fe(NO_3)_3.9H_2O$ (8.08 g). Concentration of precursor solutions were checked and optimized by ICP–AES analysis. Detailed synthesis procedures are depicted in figure 1.

2.3 *Characterization of photocatalysts*

Crystallite size and crystalline phase of praseodymium ferrite samples were determined by X-ray powder diffraction (XRD) using Rigaku Miniflex II Desktop X-ray diffractometer with Cu Kα radiation source at 30 kV and 15 mA, following a scanning rate of 5°/min. XPS measurements were performed to study oxidation states and other details of materials, by using Sigma-Probe with mono-chromated Al Kα source. Deconvolution of core level spectra was performed by using Peakfit software. The BET surface area analysis was performed by N_2 adsorption/desorption at 77 K using Micromeritics USA ASAP 2000 surface area analyser. Micro-structural and morphological properties of these materials were studied by scanning electron microscope (SEM) model JOEL JSM-6380 and high resolution transmission electron microscope (HRTEM) model JOEL JEM-3010 operated at 300 kV. Infrared spectrum was recorded on PE Spectrum-1FTIR spectrophotometer. UV-Visible diffuse reflection spectrum (UV-DRS) was obtained by Perkin-Elmer Lambda 900 spectrophotometer, equipped with an internal sphere, while $BaSO_4$ was used as reference material.

2.4 *Photocatalytic evaluations*

Deionized water (20 ml) was used for experiment after boiling, to remove dissolved gases. It was then cooled and to it optimized dose of photocatalyst praseodymium ferrite was added, followed by addition of ethanol (1 ml), and ~0.095 mg of platinum (0.0002 M) as

co-catalyst. The reactor was then fixed with a condenser, which was further attached to a gas collector. The whole experimental set-up was evacuated by using vacuum pump to remove air. The solution was continuously stirred using magnetic stirrer for uniform dispersion of catalyst. The glass reactor was illuminated with two 200 W tungsten light sources. After the predetermined period of reaction, the gas collector was closed and removed from the set-up and then evaluated on the GC equipped with molecular sieve 5A column and thermal conductivity detector (TCD). The above procedure was also followed to carry out the reaction under varying conditions of catalyst dose, illumination intensity, duration, and activity of photocatalyst was thus optimized. (Further details are provided in ref.[23])

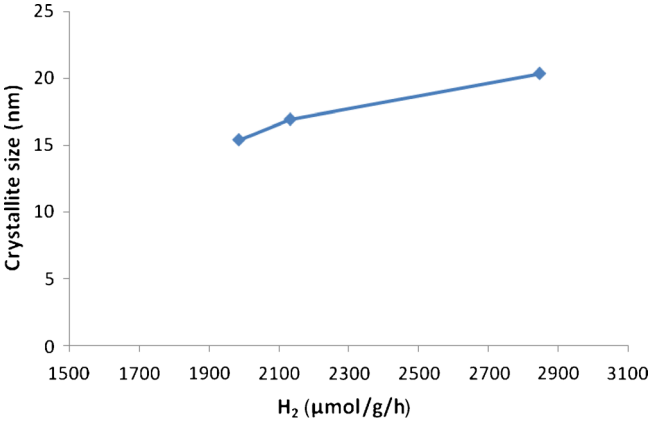

Figure 3. Correlation of crystallite size vs. hydrogen generation for $PrFeO_3$ perovskite synthesized by sol-gel, chitosan template and combustion methods.

3. Results and discussion

3.1 *Characterization of praseodymium ferrite photocatalyst*

XRD pattern of sol–gel synthesized photocatalyst is shown in figure 2a. It illustrates well-indexed diffraction peaks, clearly inferring the formation of $PrFeO_3$ type compound (Pearson's Crystal Data sheet No.1818270).[28] All the peaks could be indexed to orthorhombic cell associated with space group pbnm (62). Crystallite size of $PrFeO_3$ has been determined by using Debye–Scherer formula.

$$d = k.\lambda/\beta.\cos\theta,$$

where 'd' is the crystallite size in Å, 'k' crystallite shape factor, 'λ' is X-ray wavelength (1.5418 Å for Cu Kα), β is the width of diffraction peak and θ is the observed peak angle (degree).

The sample prepared by combustion synthesis method shows small intensity impurity peaks for Pr_6O_{11}, while sample prepared by chitosan template route shows good purity. The observed crystallite size for $PrFeO_3$ perovskite synthesized by sol–gel, template and combustion methods are 20, 17 and 15 nm, respectively, thereby, suggesting formation of nanocrystallite phases, possibly due to moderate temperature used in the synthesis. Crystallite size of all the synthesized $PrFeO_3$ photocatalysts were calculated for the obtained crystalline pure reflection (100 peak). All these praseodymium ferrite samples were calcined at 700°C, which is considered as relatively lower temperature for perovskites synthesis.

A correlation was attempted between the crystallite size and amount of hydrogen generation as shown in figure 3. Increase in crystallite size of the photocatalyst appears to show slightly increased hydrogen generation; however, this cannot be solely responsible for such an effect. BET surface area values were found to be 10.88, 15.7 and 10.13 m^2/g, for $PrFeO_3$ synthesized by sol–gel, template and combustion methods, respectively. These surface area values are reasonably high considering the synthesis temperature used. In this way, these synthesis methods result in improved physical properties of $PrFeO_3$, which are important for catalytic, photocatalytic and other surface reactions. Initial screening of different materials reveals higher hydrogen generation for the sample prepared by sol–gel method. Considering this higher photocatalytic activity and purity of sample, further characterization studies were carried out only for sol–gel prepared sample.

XPS study was carried out to determine the chemical environment and oxidation states of elements in sol–gel synthesized $PrFeO_3$. The deconvoluted X-ray photoelectron spectra of $PrFeO_3$ sample for O1s, Fe2p and Pr3d are illustrated in figure 4. Binding energy peaks for O1s was observed at 532.08, 529.9 and 528.4 eV, which correspond to different chemical states of oxygen.[22,29] The XPS signal for O1s attributed to the crystal lattice oxygen was observed at 528.4 eV, owing to contribution of Pr-O and Fe-O bonds in $PrFeO_3$ crystal lattice. Peak position at 529.9 eV was assigned for surface oxygen, which is because of hydroxyl/carbonates groups. While, the peak at 532.08 eV was attributed to surface coordinated water molecule.[30–32] The BE values for $Fe2p_{3/2}$ and $Fe2p_{1/2}$ in $PrFeO_3$ were observed at 710.9 and 723.9 eV, respectively.[33] The peak observed at 718.4 eV was reported as $Fe2p_{3/2}$ satellite peak as per NIST XPS database. These values for Fe2p confirm oxidation state of +3 for iron in the synthesized material. Similarly, for Pr3d5/2 and Pr3d3/2 in $PrFeO_3$, BE values were

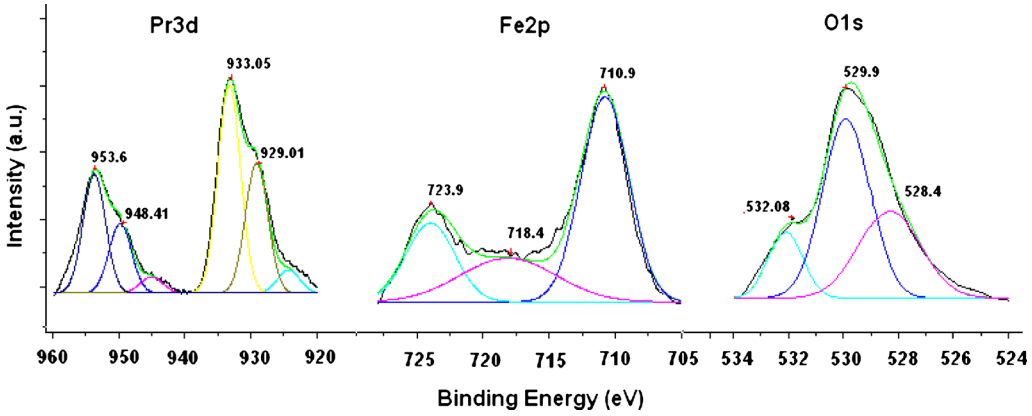

Figure 4. XPS spectra of $PrFeO_3$ perovskite.

observed in the range of 929.01–953.6 eV along with the satellite peaks. Hence, XPS study inferred that the Pr and Fe in the present $PrFeO_3$ sample are present close to common oxidation states (+3) of these elements, as represented in Pr_2O_3 and Fe_2O_3, respectively. However, deconvolution of Pr3d spectra reveals that Pr exists as Pr3+ (929.01 and 948.41 eV) as well as Pr4+ (933.05 and 953.6 eV) states in $PrFeO_3$. Thus, presence of perovskite compositions with a small amount of additional oxygen ($PrFeO_{3+\delta}$) due to this effect cannot be ruled out.[33,34]

SEM images of $PrFeO_3$ sample (figure 5) show platelet agglomerates. The image also shows that the size of the particles is not uniform; however, the surface of particles appears reasonably smooth. HRTEM images (figure 6) of synthesized $PrFeO_3$ sample show particle size in a range of 10–50 nm, further agglomerated to form larger particles as also seen in SEM images. Crystalline facets with ordered arrangements can be clearly seen with lattice width measurements. According to ICCD-PDF 47-0065, HRTEM images also infer orthorhombic symmetry of $PrFeO_3$ crystalline phase. In this way, the XRD and HRTEM studies unambiguously confirm the formation of good crystalline pure phase $PrFeO_3$. HRTEM pictures suggest nanocrystallites as well as small particle agglomerates formed

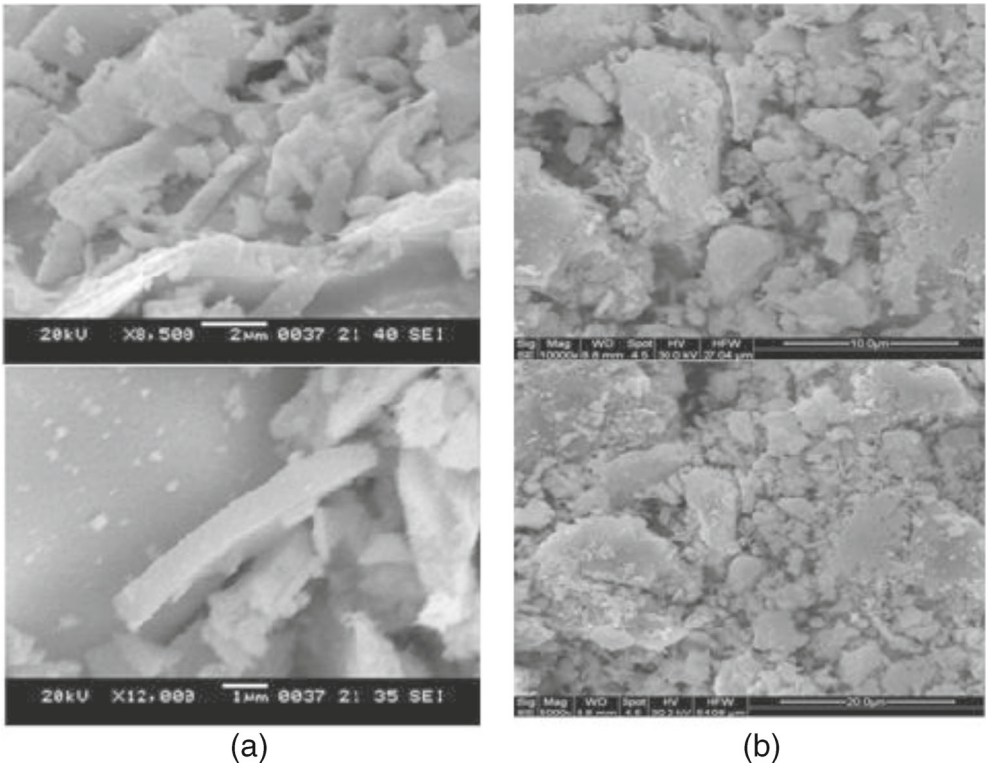

Figure 5. Scanning electron micrographs of $PrFeO_3$ synthesized by sol–gel method (**a**) and combustion method (**b**).

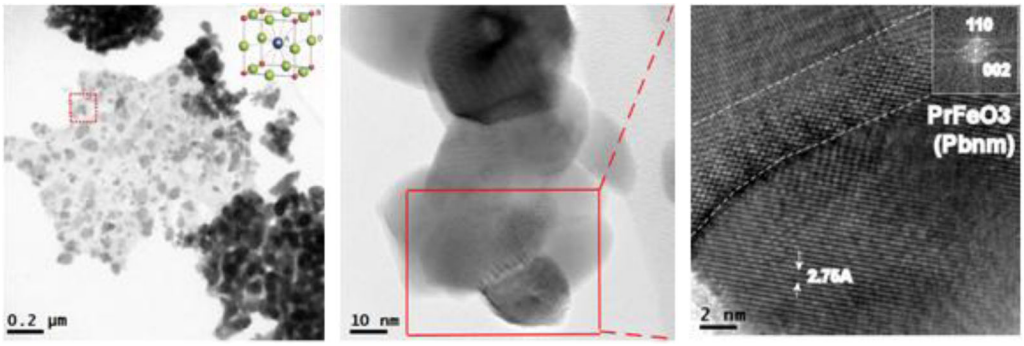

Figure 6. HRTEM images of $PrFeO_3$ perovskite.

through interconnected crystallites; thereby, suggesting low particle sintering in this sample prepared by sol–gel method.

The FTIR spectrum of sol–gel synthesized $PrFeO_3$ photocatalyst shows strong absorption bands at 454.79 cm^{-1} and 542.18 cm^{-1} and a few weak intensity bands in the range of 1300–1500 cm^{-1}. Absorption at 454.79 nm corresponds to O-Fe-O bending vibrations, while that observed at 542.18 cm^{-1} corresponds to Fe-O stretching vibration as shown in figure 7. Very weak bands were observed in 1300–1500 cm^{-1} region, which can be attributed to the formation of carbonate due to chemisorption of ambient CO_2 over the surface of catalyst.

Figure 8 shows the UV-DRS spectra of $PrFeO_3$ samples synthesized by using different methods. The band gap value estimated is 2.08 eV for $PrFeO_3$ photocatalyst synthesized by sol–gel method, as calculated by using the formula.

$$\text{Band gap (eV)} = \frac{1240}{\lambda_g}\text{nm}, \quad [35]$$

where λg is the absorption wavelength value obtained from the UV-DRS spectra.

Similarly, band gap values are also calculated for $PrFeO_3$ photocatalyst synthesized by template and combustion methods (figure 8), and the values obtained

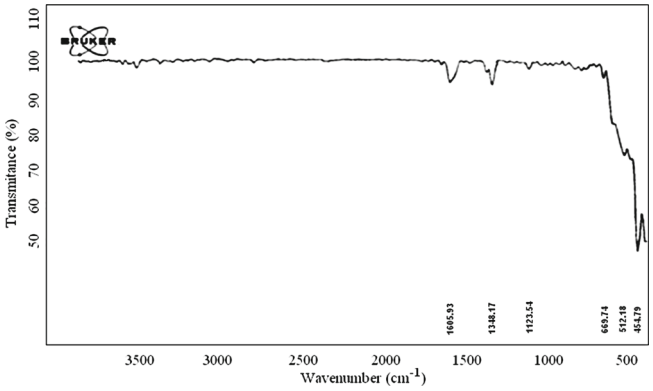

Figure 7. FTIR spectrum of $PrFeO_3$ perovskite.

are 2.03 and 1.88 eV, respectively. All the synthesized $PrFeO_3$ photocatalyst samples thus show band gap suitable for absorption of visible region of light spectrum, while the band gap values for sol–gel and template methods are better in case of desired band gap energy required for the photocatalytic water-splitting reaction.

3.2 *Photocatalytic activity*

These photocatalysts have been evaluated for their activity towards hydrogen generation through water-splitting in visible light irradiation (tungsten source) by using Pt as co-catalyst and ethanol as a sacrificial donor. Amount of hydrogen generated is 2847, 2132 and 1986 $\mu mol.h^{-}1.g^{-1}$ for photocatalyst synthesized by sol–gel, template and combustion methods, respectively. Sol–gel synthesized photocatalyst thus shows relatively higher yield of hydrogen among all the $PrFeO_3$-based photocatalysts synthesized by various routes. The $PrFeO_3$ photocatalyst synthesized by combustion route shows lower surface area and smaller band gap. This along with impurity phases could be responsible for relatively lower hydrogen generation. However, due to impurity phases, this cannot be interpreted reliably. The sol–gel synthesis route possibly provides proper conditions for present perovskite synthesis due to gelation as intermediate step. Gelation of multi-components provides controlled stoichiometry and results in good crystalline pure phase, leading to improved photocatalytic activity with higher hydrogen generation. Impurity phases can also contribute towards electron-hole recombination, leading to suppressed photocatalytic activity. Chitosan template method improves the surface area however, irregular morphology (figure 5b) of this material could also lead to increased electron-hole recombination, and thus a relatively lower photocatalytic activity. So among all the samples, the sol-gel-synthesized $PrFeO_3$ sample shows high purity and crystallinility even at relatively lower synthesis temperature of 700°C. This material

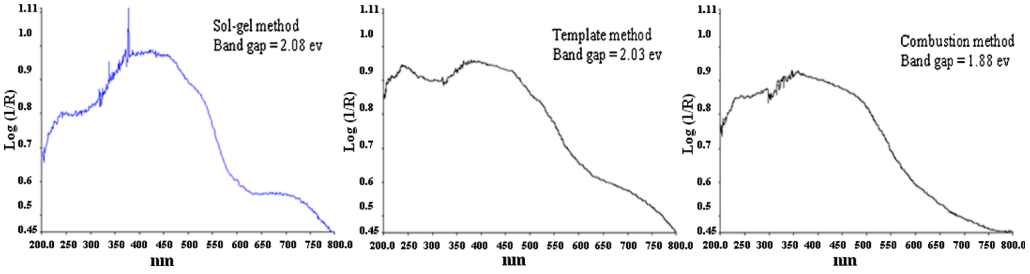

Figure 8. UV-DRS absorption spectrum of $PrFeO_3$ photocatalysts.

incidentally also shows higher value of photocatalytic hydrogen generation. The weight normalized photocatalytically generated hydrogen for $PrFeO_3$ photocatalyst (sol–gel) was 2847 μmol.g^{-1}.h^{-1} at 1 mg dose of photocatalyst. To the best of our knowledge, $PrFeO_3$ perovskite has so for not been explored for photocatalytic hydrogen generation and offers good possibility to study the impact of slightly different chemical environment than $LaFeO_3$ and other similar materials. Actual yield under the experimental condition was maximum for 10 mg photocatalyst dose, while there was a decline in hydrogen generation beyond this dose, possibly due to the blocking of light in rather concentrated suspension. The sol-gel-prepared $PrFeO_3$ shows relatively annealed morphology and smooth surface in SEM observations. Such thermal annealing or sintering is expected to reduce the defects in highly crystalline perovskite particles, thereby resulting in less number of sites for electron-hole recombination on photocatalyst surface. Electron-hole recombination is often recognized as one of the limitations in such semiconductor photocatalysts and thus could be correlated with enhanced photocatalytic activity of $PrFeO_3$ photocatalyst prepared by sol–gel route. The following investigations were carried out to study the effect of dose, sacrificial donor, co-catalyst and illumination intensity for optimization of hydrogen yield for sol-gel-synthesized $PrFeO_3$ photocatalyst.

3.2a *Effect of photocatalyst dose*: The effect of $PrFeO_3$ dose on photocatalytic hydrogen generation is shown in figure 9. Photocatalyst dose was varied from 1–30 mg keeping other parameters constant. Although, total yield of hydrogen increased with higher dose, amount of hydrogen generation after normalizing weight of photocatalyst was observed to decrease with increasing dose of $PrFeO_3$. This could be mainly due to obstruction of light by the small particles of photocatalyst at higher dose, which leads to relatively inefficient use of photocatalytic sites thus resulting in decrease of hydrogen generation per unit mass of photocatalyst used. Maximum yield in absolute term of hydrogen was observed for 10 mg dose (615.05 μmol.g^{-1}.h^{-1}), which should be considered as optimized photocatalyst dose for higher hydrogen yield.

3.2b *Effect of reaction time*: Rate of hydrogen generation by donor-assisted water-splitting reaction using $PrFeO_3$ photocatalyst was followed as a function of time. Hydrogen generation in terms of μmol.g^{-1} of photocatalyst increases as a factor of time (figure 10) until 4 h, and subsequently starts declining. This effect is discussed in the following section.

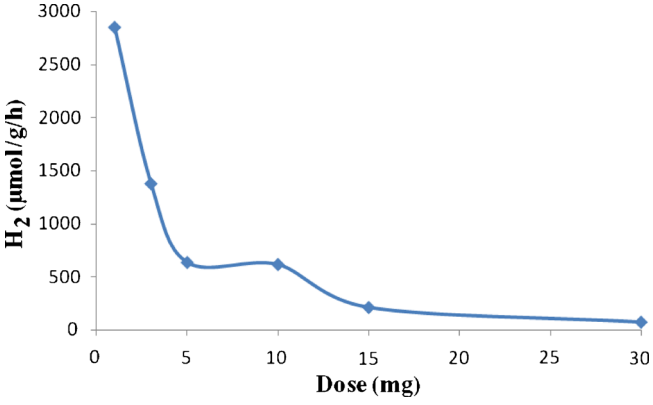

Figure 9. Effect of dose variation on hydrogen generation.

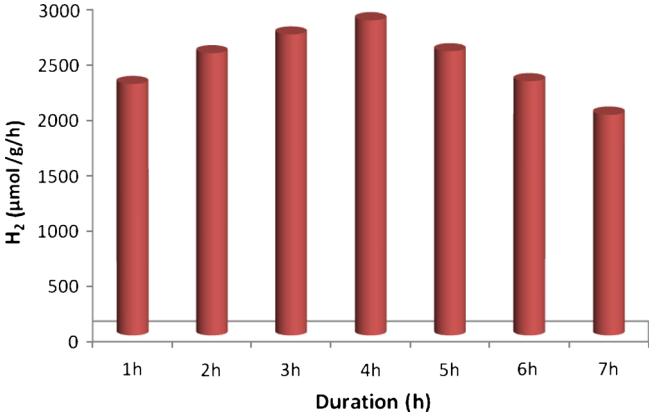

Figure 10. Kinetic study of $PrFeO_3$ photocatalyst for hydrogen generation.

4. Mechanistic aspects

A photocatalyst should have a band gap higher than 1.23 eV, which is a theoretical minimum band gap,[11] required to generate adequate energy for photocatalytic water-splitting reaction. In addition, other factors related to recombination of electron-holes, transfer of photoelectron to surface and its utilization at reduction site govern the overall activity for hydrogen generation. The $PrFeO_3$ (sol–gel) shows a potential band gap of 2.08 eV, which falls within appropriate range. When light energy greater than band gap is incident on the surface of $PrFeO_3$ photocatalyst, photoexcited electrons and holes are generated. These photogenerated electrons and holes then migrate to the surface of $PrFeO_3$ photocatalyst. Water adsorbed on the surface of photocatalyst is reduced and oxidized by electrons and holes to generate hydrogen and oxygen, respectively (figure 11). Co-catalyst Pt is used in solution form and added to reaction mixture in the present experiments. The Pt is expected to get photoreduced and deposited on photocatalyst surface as reported by several researchers.[36–38] These platinum sites then facilitate generation of molecular hydrogen after reduction of H^+ ions generated through photocatalytic reaction. Initial slow kinetics of the reaction could be due to photo-deposition of Pt on photocatalyst surface, while decrease in hydrogen yield after 4 h was due to exhaustion of sacrificial donor mainly through evaporative losses associated with evaluation system. Ethanol acts as sacrificial donor, which constantly replenishes electrons to the valance band (VB), which ultimately helps in continuation of hydrogen generation activity. Source of hydrogen generation is unlikely to be only ethanol, as experiments performed with pure ethanol (without water) do not show any measurable hydrogen. At the same time, the photocatalyst shows negligible hydrogen generation in absence of ethanol, thus suggesting that the present reaction is 'ethanol-assisted photocatalytic water-splitting' with ethanol acting as a sacrificial donor. In this way, the present $PrFeO_3$ photocatalyst appears to follow a typical semiconductor type mechanism as also observed in case of other similar perovskite compositions.

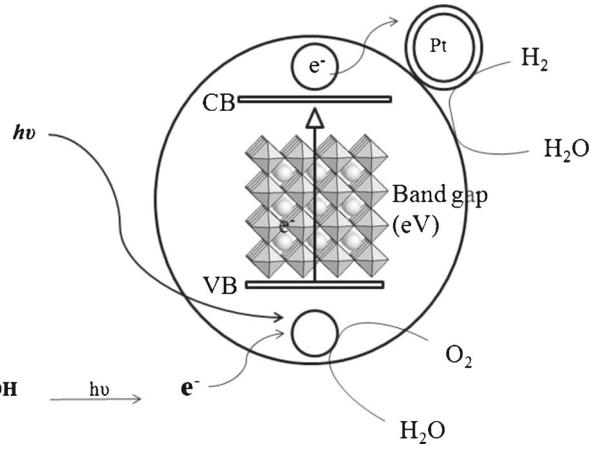

Figure 11. Photocatalytic mechanism of hydrogen generation for $PrFeO_3$ photocatalyst.

Overall hydrogen generation for $PrFeO_3$ was observed to be slightly higher than that for $LaFeO_3$ photocatalyst, which could be due to nanocrystallites (about 20 nm as compared to 39 nm for $LaFeO_3$) of synthesized perovskites. Highly crystalline perovskite phase with relatively annealed surface with less defects might as well contribute to higher hydrogen generation activity as surface defects are often correlated with increased electron-hole recombination.

5. Conclusion

Iron-based mixed oxides including that of perovskite and other structures are attracting more attention for a variety of catalytic reactions. This is due to the low cost, abundance and environmental safety-related advantages. Iron similar to many other transition metals shows significantly altered catalytic properties in different chemical environments and is therefore interesting to study. Our recent study on ferrite type photocatalyst has prompted us to explore the present composition of $PrFeO_3$ with almost similar structure and other properties, except for some difference in oxidation states and electronic structure. In the present study, praseodymium ferrite was synthesized at 700°C by using sol–gel, template and combustion methods to compare their properties. Sol–gel method of synthesis offers good crystallinity, purity, nanocrystalline nature and suitably anisotropic phase formation. The $PrFeO_3$ type photocatalysts thus synthesized were characterized by *p*-XRD, BET-SA, SEM, HRTEM, XPS, FTIR and UV-DRS techniques, suggesting improved surface area with different purity depending on method of synthesis. These studies infer formation of single phase perovskite type crystalline compound with orthorhombic structure having crystallite size as small as 20 nm by sol–gel method; thereby, confirming the nanocrystalline nature of $PrFeO_3$ perovskite. The XPS study also supports Fe-O bond formation in synthesized $PrFeO_3$ photocatalyst. The UV-Vis diffuse reflectance spectroscopic analysis exhibited an optical band gap of approximately 2.08 eV, which was corroborated by photocatalytic activity for hydrogen generation under visible light irradiation. This is an interesting finding as such a

material could be potential source of visible light photocatalytic activity. A reasonably high H_2 generation of 2847 μmol.g^{-1}.h^{-1} was observed under optimized conditions in visible light irradiation and using ethanol as sacrificial donor with Pt as reducing site. It is possible to photo-reduce and deposit Pt as a co-catalyst on this perovskite material *in situ*, which then acts as reducing sites for molecular hydrogen generation. Such perovskite type semiconductor compositions are usually very stable and therefore add to the list of existing potential photocatalysts as well as suitable matrices for synthesis of hetero-junction type photocatalyst compositions. Efforts on their synthesis and photocatalytic evaluations are underway.

Acknowledgements

This study was supported by Network Project TAPSUN (No. NWP 56) sponsored by the Council of Scientific and Industrial Research (CSIR), New Delhi, India as well as under the bilateral project between CSIR and Academy of Sciences of the Czech Republic. Material characterization and interpretation was carried out under research cooperation between CSIR-NEERI and NIMS, Japan.

References

1. Currao A 2007 Transformation and energy storage of solar energy **61** 815
2. Lu T and Barbir F 2008 *Int. J. Hydrogen Energy* **17** 391
3. Intermediate energy infobook, 2008, 30
4. Deluga G, Salge J, Schmidt L and Verykios X 2004 *Science* **303** 993
5. Dai X, Wu Q, Li R, Yu C and Hao Z 2006 *J. Phys. Chem.* **B110** 25856
6. Park W and Moon I 2007 *Biochem. Eng. J.* **36** 19
7. Guo L, Zhao L, Jing D, Lu Y, Yang H, Bai B, Zhang X, Ma L and Wu X 2009 *Energy* **34** 1073
8. Navarro R, Sanchez M, Alvarez-Galvan M, Valle F and Fierro J 2009 *Energy Environ. Sci.* **2** 35
9. Nowothy J, Bak T, Nowotny M and Shepprd L 2006 *J. Phys. Chem.* **B110** 18492
10. Kudo A and Miseki Y 2009 *Chem. Soc. Rev.* **38** 253
11. 11. Oudenhoven J F M, Scheijen F J E and Wolffs M 2004 *Chemistry of catalytic system 2: Photocatalysis*
12. Fukumoto S, Kitano M, Takeuchi M, Matsuoka M and Anpo M 2009 *Catal. Lett.* **127** 39
13. Wang F, Liu C, Liu C, Chao J and Lin C 2009 *J. Phys. Chem.* **C133** 13832
14. Li Y, Xie Y, Peng S, Lu G and Li S 2006 *Chemosphere* **63** 1312
15. Chen X, Shen S, Guo L and Mao S 2010 *Chem. Rev.* **110** 6503
16. Lo C, Huang C, Liao C and Wu J 2010 *Int. J. Hydrogen Energy* **35** 1523
17. Lee J, Hwang D, Reddy V, Kim J, Oh S and Li W *Optimization of layered perovskite materials as a photocatalyst for photocatalytic water splitting*
18. Weidenkaff A 2004 *Adv. Eng. Mater.* **6** 709
19. Tanaka H and Misono M 2001 19. *Current option in solid state Mater. Sci.* **5** 381
20. Wei Y, Li J, Huang Y, Huang M, Lin J and Wu J 2009 20. *Solar Energy Material and Solar Cell* **93** 1176
21. Dom R, Subashri R, Radha K and Borse P 2011 *Solid State Commun.* **151** 470
22. Parida K, Reddy K, Martha S, Das D and Biswal N 2010 *Int. J. Hydrogen Energy* **35** 12161
23. Borse P H 2009 *J. Korean Phys. Soc.* **55** 1472
24. Han S, Kang T, Joo O and Jung K 2007 *Solar Energy* **81** 623
25. Tijare S, Joshi M, Padole P, Manglurkar P, Rayalu S and Labhsetwar N 2012 *Int. J. Hydrogen Energy* **37** 10451
26. Arakawa T, Tsuchi S and Shiokawa J 1982 *J. Catal.* **74** 317
27. Guo L, Huang K, Chen Y, Li G, Yuan L, Peng W, Yuan H and Feng S 2011 *J. Solid State Chem.* **184** 1048
28. Aleksovska S, Dimitrovska S and Kuzmanovski I 2007 *ACSLE7* **54** 574
29. Pandey S K, Bindu R, Bhatt P, Chaudhari S M and Piple A V 2005 *Physica B* **365** 47
30. Ito A, Masumoto H and Goto T 2006 *Mater. Trans.* **11** 2808
31. Dupin J, Gonbeau D, Vinatire P and Levasseur A 2000 *Phys. Chem. Chem. Phys.* **2** 1319
32. Ponce S, Pena M A and Fierro J L G 2000 *Appl. Catal. B: Environ.* **24** 193
33. Pradhan G and Parida K 2010 *Int. J. Engg. Sci. Tech.* **2** 53
34. Kimura S, Arai F and Ikezawa M 1996 *J. Electron Spectrosc. Relat. Phenom.* **78** 135
35. Joshi M, Labhsetwar N, Manglurkar P, Tijare S, Kamble, S and Rayalu S 2009 *Appl. Catal. A: Gen.* **357** 26
36. Dehouche F, Archirel P, Remita H, Brodie-Linder N and Traverse A 2012 *RSC Adv.* **2** 6686
37. Tacconi N R, Rajeshwar K, Valluri W C V, Wampler W A, Lin W Y and Nikiel L 2010 *J. Electrochem. Soc.* **157** B147
38. Bittencourt C, Hecq M, Felten A, Pireaux J J, Ghijsen, J, Felicissimo M P, Rudolf P, Drube W, Ke X and Tendeloo G V 2008 *Chem. Phys. Lett.* **462** 260